

ClimaOoD: Improving Anomaly Segmentation via Physically Realistic Synthetic Data

Yuxing Liu Yong Liu
Beijing University of Chemical Technology



Figure 1. Visual comparison of dataset limitations and ClimaOoD. (a) Existing datasets suffer from limited weather and scene diversity. (b) Recent data synthesis leads to contextual inconsistencies and physically unrealistic object placement. (c) ClimaDrive generates diverse weather scenes and places anomalies with realistic spatial arrangement, using semantic maps and text prompts for better OoD object placement.

Abstract

Anomaly segmentation seeks to detect and localize unknown or out-of-distribution (OoD) objects that fall outside predefined semantic classes—a capability essential for safe autonomous driving. However, the scarcity and limited diversity of anomaly data severely constrain model generalization in open-world environments. Existing approaches mitigate this issue through synthetic data generation, either by copy-pasting external objects into driving scenes or by leveraging text-to-image diffusion models to inpaint anomalous regions. While these methods improve anomaly diversity, they often lack contextual coherence and physical realism, resulting in domain gaps between synthetic and real data. In this paper, we present ClimaDrive, a semantics-guided image-to-image framework for synthesizing semantically coherent, weather-diverse, and physically plausible OoD driving data. ClimaDrive unifies structure-guided

multi-weather generation with prompt-driven anomaly inpainting, enabling the creation of visually realistic training data. Based on this framework, we construct ClimaOoD, a large-scale benchmark spanning six representative driving scenarios under both clear and adverse weather conditions. Extensive experiments on four state-of-the-art methods show that training with ClimaOoD leads to robust improvements in anomaly segmentation. Across all methods, AUROC, AP, and FPR95 show notable gains, with FPR95 dropping from 3.97 to 3.52 for RbA on Fishyscapes LAF. These results demonstrate that ClimaOoD enhances model robustness, offering valuable training data for better generalization in open-world anomaly detection.

1. Introduction

Anomaly segmentation aims to detect out-of-distribution (OoD) objects not predefined, serving as a complementary capability to semantic segmentation methods[3, 18, 20, 25, 30]. This capability is crucial for safety-critical applications such as autonomous driving, where models must respond reliably to unexpected hazards like fallen cargo, construction equipment, or animals on the road[8, 11, 12, 40]. Despite notable advances in deep segmentation networks, their performance in open-world environments remains highly constrained by the availability and diversity of anomaly data[3, 5, 6, 10, 18, 29, 38].

In the real world, anomalous events are inherently rare and unpredictable, which makes collecting large-scale, high-quality anomaly data for training anomaly segmentation models extremely difficult[3, 26, 38, 43]. Existing benchmarks often focus on urban streets under clear weather, overlooking complex environmental conditions (e.g., tunnels, highways, rain, fog, or snow)[3, 6, 18, 29] (see Figure 1.a). Consequently, models trained on these datasets struggle to generalize when faced with unseen weather or novel environments[30, 43].

To alleviate the scarcity of anomaly data, recent state-of-the-art methods have explored two main paradigms of synthetic data generation. The first is the copy-paste approach [20, 25, 45], which crops objects from external datasets (e.g., COCO [17], ADE20K [47]) and pastes them into driving scenes (e.g., Cityscapes [9]) to simulate OoD events. The second leverages text-to-image diffusion models [22, 38], where masked regions in driving images are filled with anomalous objects guided by textual prompts. While both approaches enrich anomaly diversity, they remain limited in complementary ways: copy-paste methods struggles to maintain **contextual consistency**, often causing significant discrepancies in brightness and color between pasted objects and backgrounds. Meanwhile, text-to-image diffusion-based approaches lack **physical realism**, leading to implausible object placement regarding positional coherence and scale (see Figure 1.b). These issues create domain gaps between synthetic training data and real-world application scenarios, ultimately compromising model robustness and generalization capability.

In fact, the image-to-image paradigm effectively mitigates contextual inconsistencies between inserted objects and surrounding scenes through its encoding-decoding process. Moreover, guided by semantic priors, it enables the generation of objects with appropriate location and scale, thereby adhering to physical constraints. Inspired by these observations, we propose ClimaDrive, a unified, semantics-guided image-to-image framework that redefines OoD data synthesis. Unlike previous methods that heuristically inject anomalies or rely on unconstrained inpainting, ClimaDrive integrates perspective-aware spatial con-

straints and semantics-consistent scene rendering directly into the generation process. This approach combines structural priors (e.g., road geometry, depth cues) with semantic distribution constraints to place anomalies accurately in context, ensuring both realistic spatial placement and physical plausibility. The multi-scene weather generator further enhances ClimaDrive by simulating diverse weather conditions (e.g., rain, snow, fog), improving environmental realism and producing semantically consistent, visually varied driving scenes—capabilities that prior methods cannot achieve.

Built upon ClimaDrive, we construct ClimaOoD, a large-scale benchmark collected to evaluate anomaly segmentation robustness in open-world conditions. ClimaOoD synthesizes over 10,000 image-mask pairs across multiple weather conditions (clear, rain, fog, snow, cloudy, night-time) for training. After careful curation, we create a refined test set of 1,200 image-mask pairs, covering six distinct driving scenarios (e.g., city streets, highways, tunnels) and 93 anomaly types. In comparison to existing anomaly segmentation benchmarks such as LostAndFound [29] (1 landform, 9 anomaly types), Fishyscapes [3] (1 landform, 7 anomalies), and SMIYC-RoadAnomaly21 [6] (4 landforms, 26 anomalies), ClimaOoD provides substantially broader coverage with 6 landforms, 93 anomaly categories, and 6 distinct weather conditions. This wide diversity ensures more robust training for anomaly segmentation models under varied open-world conditions.

We conducted comprehensive experiments on ClimaOoD by training four state-of-the-art anomaly segmentation methods on our constructed training dataset and testing them on our filtered test set. Quantitative results demonstrate that incorporating ClimaOoD into training robustly improves anomaly segmentation performance. Across four state-of-the-art methods, AUROC increases by 0.66%, and AP improves by 3.25%. However, when evaluated under adverse conditions, models still show robustness gaps, with the average FPR95—rising from 7.8% in clear weather to 11.0%, underscoring the need for more realistic OoD data to improve generalization in open-world anomaly detection. Our contributions are summarized as follows:

- We build ClimaOoD, a comprehensive benchmark encompassing six representative driving scenarios across diverse weather conditions, including clear, foggy, rainy, and snowy environments. It contains over 10,000 high-fidelity image-mask pairs.
- We propose ClimaDrive, a semantics-guided image-to-image framework that generates realistic anomalous driving scenes.
- Extensive experiments show that training with ClimaOoD improves performance across four state-of-the-art methods, boosting average AP by 3.25% and enhancing model precision and recall across diverse scenes.

2. Related Work

2.1. Anomaly Segmentation Benchmarks in Autonomous Driving

Anomaly segmentation relies heavily on high-quality and diverse datasets[18, 33, 43, 45]. Yet real-world anomaly collection remains difficult—anomalous events are rare, unpredictable, and highly variable across environments[21, 46]. This scarcity limits model generalization to diverse out-of-distribution (OoD) scenarios[14, 35, 48].

Early benchmarks such as LostAndFound[29] and Fishyscapes[3] focus mainly on clear-weather urban scenes, offering limited anomaly and scene diversity. RoadAnomaly[18] and SMIYC[6] expand scene types and weather conditions but remain small in scale. ComsAmy[38] increases scenario and weather coverage yet contains only 468 images, restricting robust evaluation. Overall, existing datasets are too limited or too small to reflect the complexity of real-world driving environments.

These limitations underscore the need for a large-scale, diverse benchmark that spans varied scenarios, weather conditions, and anomaly types—providing a more realistic foundation for developing and evaluating anomaly segmentation models under open-world conditions.

2.2. Synthetic Data Generation Methods

In anomaly segmentation, generating synthetic data has become a crucial strategy to overcome the limitations of real-world datasets[19, 33, 36, 37]. Two primary methods have been widely adopted: the *copy-paste* approach and *text-to-image diffusion models*.

The *copy-paste* method inserts objects from external datasets into driving scenes[20, 21, 25, 36], as used in Fishyscapes-Static[3] and StreetHazards[34]. While it enables easy anomaly diversification, it often breaks contextual consistency—pasted objects frequently mismatch scene geometry, scale, or lighting. *Text-to-image diffusion* synthesizes anomalies directly via prompts[16, 22, 27, 28]. Loiseau et al.[22], for instance, generate anomalies from randomly sampled boxes. Despite improved visual diversity, these methods lack physical grounding, leading to spatially or geometrically misaligned anomalies.

Overall, existing synthetic approaches enhance diversity but still struggle to ensure semantically coherence and physical realism, motivating the need for a more unified and physically consistent generation framework.

3. The ClimaOoD Dataset

This section introduces the proposed **ClimaDrive** framework and the resulting **ClimaOoD** dataset. We first detail the data generation methodology, including the synthesis of realistic multi-weather scenes and physically consistent anomalies. Then, we present the composition and statistics

of ClimaOoD, highlighting its scale, scenario diversity, and comprehensive weather coverage.

3.1. Generation Framework: ClimaDrive

ClimaDrive introduces a unified, semantics-guided image-to-image framework that fundamentally redefines out-of-distribution (OoD) data synthesis. Instead of heuristically injecting anomalies or relying on unconstrained inpainting, ClimaDrive enforces perspective-aware spatial validity and semantics-consistent scene rendering as first-class constraints in the generation process. This design upgrades anomaly synthesis from ad-hoc manipulation to a physically grounded generative pipeline that achieves controllable weather variation, reliable spatial placement, and scene-faithful integration—capabilities that prior approaches fundamentally cannot realize. The overall training process is illustrated in Figure 2.

Multi-scene weather generator: To enrich environmental diversity while preserving spatial structure, we generate multi-weather driving scenes conditioned on both semantics and text. Given a semantic map $S_{\text{sem}} \in \mathbb{R}^{H \times W}$, an image \tilde{I} is synthesized as: $\tilde{I} \sim p_{\theta}(I \mid S_{\text{sem}}, p)$ where p is a textual prompt describing scene attributes.

Scene attributes $\alpha = \{\alpha^{\text{weather}}, \alpha^{\text{scene}}, \alpha^{\text{time}}\}$ are derived from BDD100K[41] metadata and fused with a caption c from BLIP [15] to form $p = f(c, \alpha)$. Stable Diffusion [32] with ControlNet [24] is employed, where ControlNet is fine-tuned using S_{sem} as structural guidance and p as the linguistic condition. This preserves geometric alignment while achieving realistic variation across weather and lighting conditions.

AnomPlacer: Anomalous objects in driving scenes must respect both perspective and drivable constraints to ensure realistic placement. To address this, we first extract drivable regions R from the given semantic layout S_{sem} , and then sample N pseudo-bounding boxes $B = \{b_i = (x_i, y_i, w_i, h_i)\}$, with $N = 64$. A perspective prior is applied to adjust the scales of the boxes based on the image height H , ensuring that object size varies according to depth (i.e., the vertical position of the bounding box), as given by the equation: $h_i = \frac{H}{y_i}$, $w_i \propto h_i$. This adjustment ensures that anomalies are placed according to the perspective, maintaining physical realism.

Next, a detection backbone F_{θ} predicts the adjusted bounding boxes \hat{B} , which are supervised by Hungarian-matched pseudo boxes B . The localization loss function \mathcal{L}_{box} optimizes both the positional alignment and the intersection-over-union (IoU) between predicted and ground truth boxes:

$$\mathcal{L}_{\text{box}} = \sum_{j=1}^N \left[\|(x_j, y_j) - (\hat{x}_{\pi(j)}, \hat{y}_{\pi(j)})\|_1 + \text{IoU}(b_j, \hat{b}_{\pi(j)}) \right].$$

Table 1. Comparison of anomaly segmentation benchmarks. ClimaOoD provides broader scene coverage, richer weather diversity, and more anomaly types than existing datasets.

Dataset	Anomaly pixels	Size	Landforms	Anomalies	Weather
LostAndFound [29]	0.12%	1203	1	9	clear
Fishyscapes LAF [3]	0.23%	373	1	7	clear
SMIYC-RoadObstacle21 [6]	0.12%	327	2	31	clear, frosty, night
RoadAnomaly [18]	9.85%	60	3	21	clear
SMIYC-RoadAnomaly21 [6]	13.83%	100	4	26	clear
ClimaOoD (ours)	2.37%	1200	6	93	clear, rain, fog, snow, cloudy, night

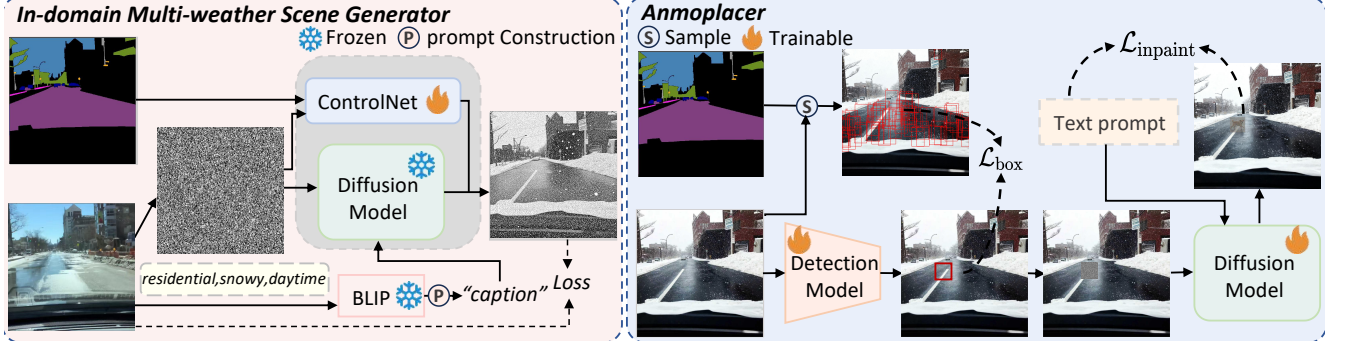


Figure 2. ClimaDrive Training Pipeline. (a) Multi-Scene Weather Generator: A structure-guided diffusion model creates semantically consistent driving scenes under diverse weather conditions using BDD100K inputs and scene-aware prompts. (b) AnomPlacer: A trainable module that predicts anomaly locations and synthesizes OoD objects via text-conditioned diffusion inpainting (e.g., “dog”).

To generate anomalous objects, we use a diffusion model for inpainting. Each predicted bounding box \hat{b}_j is filled with an anomalous object \tilde{O}_j based on the scene’s global context S_{scene} (e.g., “Tunnel, Rainy, Daytime”) and the object concept t_j (e.g., “sofa”, “dog”). The diffusion model generates an object \tilde{O}_j conditioned on the box and the scene: $\tilde{O}_j \sim p_{\theta}(O | \hat{b}_j, S_{\text{scene}}, t_j)$. This ensures that the generated objects are both semantically coherent (appropriate for the scene) and physically consistent (matching perspective and scale).

The overall objective function combines the localization loss \mathcal{L}_{box} and the inpainting loss $\mathcal{L}_{\text{inpaint}}$, which is optimized in two stages. The first stage pretrains the localization module, and the second stage refines the results through joint optimization with the inpainting model:

$$\mathcal{L}_{\text{total}} = \mathcal{L}_{\text{box}} + \mathcal{L}_{\text{inpaint}}$$

Additionally, grounding-based anomaly masks M_{ano} are generated using the Grounding-SAM method[49], and these masks are further refined using a lightweight noise-denoise process to improve boundary smoothness and coherence, ensuring that the generated anomalies align well with the scene structure.

3.2. Dataset Construction and Selection

To enable robust training and evaluation, the ClimaOoD benchmark is constructed through a two-stage process and

organized along scene–weather dimensions with consistent anomaly annotations.

First, we generate a large-scale training dataset of 10,230 synthetic images (with corresponding masks), covering 6 weather conditions (clear, rain, fog, snow, cloudy, night) and 6 driving scene types (city street, highway, tunnel, gas station, residential, parking lot). This dataset incorporates 93 anomaly categories—featuring diverse object appearances, scales, and types (e.g., animals, vehicles, obstacles)—laying a solid foundation for model training.

From this extensive training set, we curated a representative 1,200-image test set through manual screening that serves as the core of the ClimaOoD benchmark for evaluation. The selection process prioritized samples with clear semantic annotations, balanced distribution across scene-weather combinations, and realistic representation of anomalous scenarios to ensure benchmark reliability. Table 1 highlights that test set markedly broadens scene types, weather conditions, and anomaly diversity, offering a more comprehensive benchmark for evaluating open-world robustness.

Each sample includes a binary anomaly mask for pixel-level assessment. Anomalies occupy 2.37% of image pixels on average, ranging from small objects to large obstacles, and are placed in perspective-aware drivable regions to ensure realistic geometric integration.

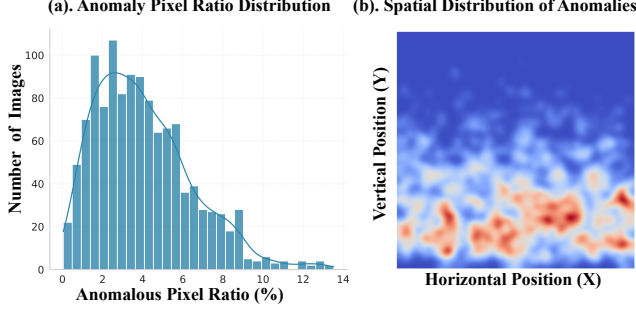


Figure 3. Anomaly pixel statistics in **ClimaOoD**: (a) Distribution of anomaly pixel fraction per image, indicating scale diversity; (b) Spatial distribution heatmap of anomaly pixels, showing that anomalies frequently appear near drivable regions.

3.3. Visualization and Statistical Analysis

The diversity and scale of ClimaOoD are further demonstrated through visual and statistical analysis. Figure 3.(a) shows the distribution of anomaly pixel fractions, highlighting the variability in the scale of anomalies, from small objects to large distractors. Figure 3.(b) presents a spatial heatmap that illustrates the concentration of anomalies in drivable areas, reflecting real-world risk zones commonly encountered in autonomous driving.

In addition, Figure 4 presents a 6×6 visualization grid, showcasing different scene and weather combinations. Each image demonstrates the fidelity and realism of ClimaOoD, with anomalies such as animals, boxes, and other objects seamlessly integrated into various weather conditions like foggy tunnels or rainy highways. This grid illustrates the effectiveness of our generation pipeline in capturing the complexity and diversity of open-world driving scenarios.

4. Experiment

Our experiments employ ClimaOoD for training and test set for benchmarking four state-of-the-art anomaly segmentation models.

Methods. These four methods represent two main paradigms in out-of-distribution (OoD) anomaly segmentation. Outlier-exposure methods (RPL[20], Mask2Anomaly[30]) aim to directly highlight abnormal regions: RPL[20] learns residual patterns to increase pixel-level sensitivity, while Mask2Anomaly[30] formulates anomaly detection as mask classification with masked attention. Uncertainty-based methods (RbA[25], UNO[10]) calibrate anomaly scores by modeling prediction confidence: RbA[25] suppresses overconfident in-distribution logits, and UNO[10] adopts a $K+1$ classifier with an explicit outlier class to refine anomaly scoring.

Evaluation Metrics. We adopt three standard OoD detection metrics: Average Precision (AP) measures overall detection accuracy, Area Under the ROC Curve (AUROC)

evaluates the model’s ability to distinguish in- and out-of-distribution pixels, and FPR95 denotes the false positive rate when the true positive rate is 95%, reflecting detection reliability.

4.1. Training OoD Segmentation Models

To assess the impact of training with the ClimaOoD dataset, we compare the performance of four state-of-the-art OoD segmentation models when trained with ClimaOoD versus original datasets. The models are evaluated on four benchmark datasets (Fishyscapes LAF[3], RoadAnomaly[18], RoadAnomaly21[6], and RoadObstacle21[6]) to examine the generalization capability under diverse driving scenarios and weather conditions.

Results and Analysis. Table 2 summarizes the performance improvements when training with ClimaOoD. Across all methods, training with ClimaOoD results in notable gains in AUROC, AP, and FPR95. For example, RbA[25] achieves an increase in AUROC from 97.19 to 97.85 on Fishyscapes LAF, and AP improves from 78.27 to 81.32 on RoadAnomaly. Similarly, Mask2Anomaly[30] sees improvements in both AUROC (from 95.41 to 96.28) and AP (from 69.46 to 74.15) across the datasets.

In particular, training with ClimaOoD enhances the robustness of these models, with FPR95 decreasing in most cases (e.g., RbA[25] drops from 3.97 to 3.52 on Fishyscapes LAF). These results demonstrate that ClimaOoD provides valuable, diverse training data that leads to better generalization and performance under a wide range of OoD conditions. The improvements highlight the significance of training with realistic, weather-diverse data for improving OoD segmentation in open-world environments.

4.2. Benchmarking OoD Segmentation Models

To evaluate the robustness of OoD segmentation methods in diverse driving environments, we benchmark four representative models on the ClimaOoD’s test set, covering various scenarios (e.g., urban streets, highways) and weather conditions (e.g., clear, adverse). All models are tested in their official form, ensuring the focus is on generalization across different environments.

Results and Analysis. Table 3 shows that all methods deteriorate under adverse weather compared with clear conditions. For example, RPL’s AUROC drops from 98.10 to 97.80 in *CityStreet*, and the largest declines appear in tunnel and nighttime scenes, where AP decreases by 3–5 points due to occlusion and low illumination.

Although UNO[10] and RPL[20] achieve the strongest overall results, all methods show clear robustness gaps in complex environments. Unlike prior benchmarks such as Fishyscapes[3]—restricted to clear-weather urban scenes—ClimaOoD exposes failure cases across diverse weather and lighting, providing a more realistic and com-

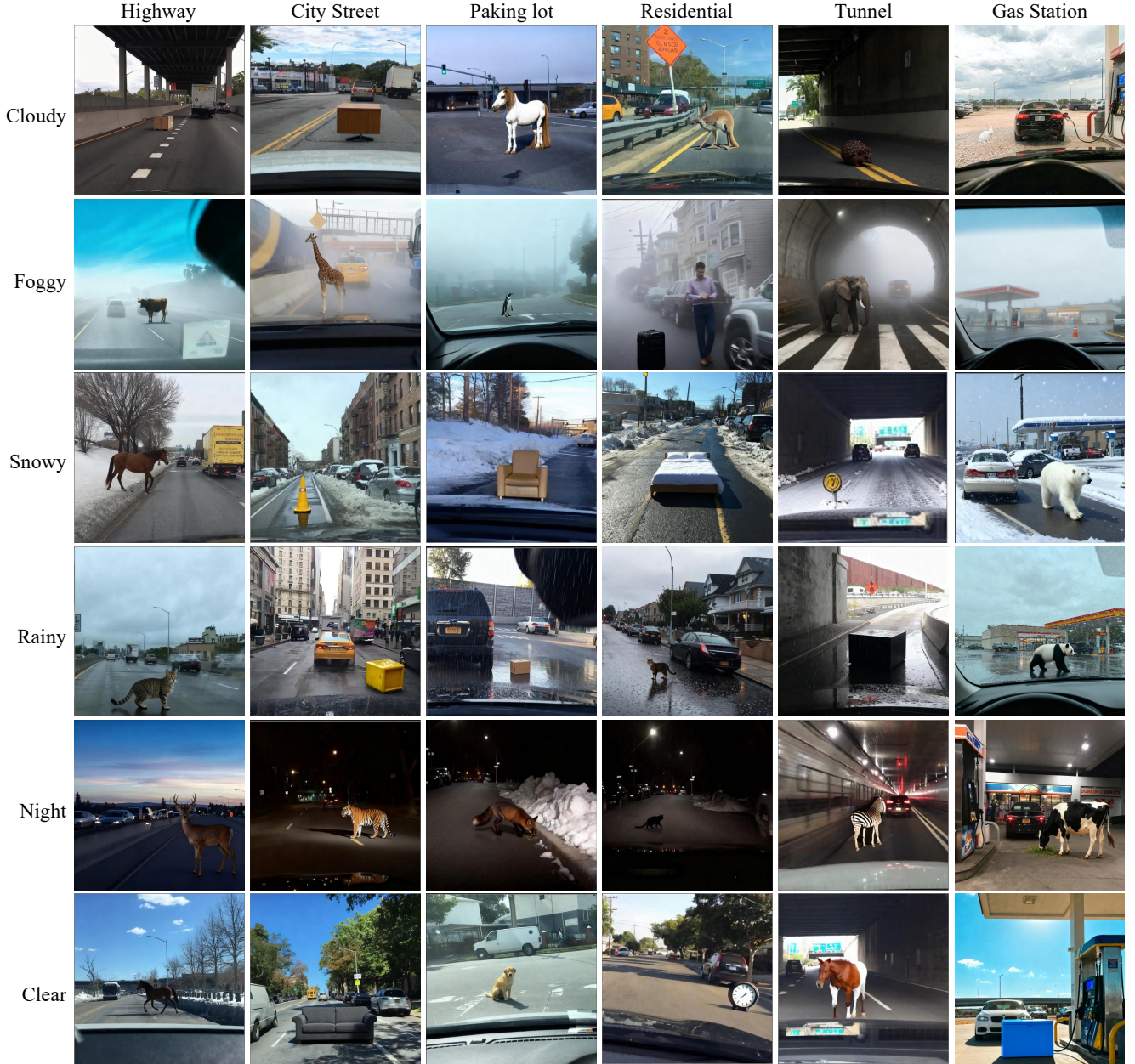


Figure 4. Visual examples from our **ClimaOoD** dataset showing synthetic anomaly scenes under diverse weather conditions. Each scene exhibits realistic illumination, texture variations, and weather-specific visual cues. Anomalous objects are seamlessly integrated into the environment, highlighting the controllable diversity and fidelity of our generation pipeline.

prehensive evaluation of OoD segmentation performance.

4.3. Ablation Studies

To assess the impact of ClimaOoD on OoD detection, we conduct ablations on SMIYC-RoadAnomaly21 and SMIYC-RoadObstacle21 using two representative methods, RbA and RPL. We compare three training configurations of equal size: (1) Original, using copy-paste and text-to-image data; (2) Clear&City Street, using clear-weather city scenes from ClimaOoD; and (3) Full ClimaOoD, using all weather conditions and driving scenarios.

Results. Table 4 shows that training on ClimaOoD (Clear) gives moderate gains, while Full ClimaOoD consistently yields the best performance. On RoadAnomaly21, RbA improves from 97.61 to 98.14 AUROC and reduces FPR95 from 8.42 to 7.35; RPL improves from 98.05 to 98.71 AUROC with FPR95 dropping from 7.22 to 5.98. On RoadObstacle21, both methods maintain high AUROC (99.8+); slight AP and FPR95 variations stem from the small object sizes in RoadObstacle21, which differ from those in our synthetic data.

Qualitative results in Figure 5 further confirm that mod-

Table 2. Comparison of OoD detection performance with and without **ClimaOoD** as training data. Results are reported in AUROC (\uparrow), AP (\uparrow), and FPR95 (\downarrow) in %. Bold indicates better performance between the two training strategies.

Method	Dataset	Original Output			Trained with ClimaOoD (Ours)		
		AUROC \uparrow	AP \uparrow	FPR95 \downarrow	AUROC \uparrow	AP \uparrow	FPR95 \downarrow
RbA[25]	FishyScape LAF	97.19	78.27	3.97	97.85	81.32	3.52
	RoadAnomaly	98.16	88.62	6.07	98.53	90.47	5.21
	RoadAnomaly21	97.61	89.39	8.42	98.14	91.26	7.35
	RoadObstacle21	99.81	98.40	0.04	99.86	97.95	0.03
RPL[20]	FishyScape LAF	99.38	70.62	2.52	99.51	75.89	2.78
	RoadAnomaly	95.72	71.60	17.75	97.26	78.93	14.32
	RoadAnomaly21	98.05	88.53	7.22	98.71	91.08	5.98
	RoadObstacle21	99.96	96.71	0.09	99.97	97.54	0.12
Mask2Anomaly[30]	FishyScape LAF	95.41	69.46	9.31	96.28	74.15	7.86
	RoadAnomaly	96.54	80.05	13.94	97.32	83.67	11.59
	RoadAnomaly21	98.93	95.49	2.39	98.87	94.96	2.18
	RoadObstacle21	99.91	92.83	0.16	99.93	95.26	0.13
UNO[10]	FishyScape LAF	96.88	74.49	6.86	97.63	80.12	5.79
	RoadAnomaly	97.71	87.21	6.88	97.54	89.76	5.42
	RoadAnomaly21	97.87	90.28	6.02	97.73	92.04	4.85
	RoadObstacle21	99.58	80.09	1.59	99.46	84.37	1.38

Table 3. OoD detection results across different **scenarios** and **weather conditions** on **ClimaOoD**. We report AUROC (\uparrow), AP (\uparrow), and FPR95 (\downarrow) for four state-of-the-art methods, with all values in percentage (%). Best results are in **bold**, second best are underlined.

Scenario	Weather	RPL [20]			RbA[25]			Mask2Anomaly[30]			UNO[10]		
		AUROC	AP	FPR95	AUROC	AP	FPR95	AUROC	AP	FPR95	AUROC	AP	FPR95
CityStreet	Clear	98.10	<u>74.00</u>	6.80	94.50	50.00	23.00	95.20	60.00	21.00	<u>98.00</u>	74.80	6.00
	Adverse	97.80	<u>72.00</u>	7.40	94.00	48.00	25.00	94.80	58.50	22.00	<u>97.60</u>	73.00	6.80
Gas station	Clear	98.00	<u>80.50</u>	11.00	94.20	52.00	21.00	95.10	61.00	20.50	<u>98.40</u>	81.50	10.20
	Adverse	97.60	<u>79.00</u>	11.80	93.80	50.00	22.50	94.70	59.00	21.50	<u>98.10</u>	80.00	11.00
Highway	Clear	98.90	<u>82.80</u>	4.50	95.00	53.00	20.00	95.50	62.00	19.50	<u>98.70</u>	83.50	<u>4.80</u>
	Adverse	98.50	<u>81.20</u>	5.00	94.20	51.00	22.00	95.20	60.50	20.50	<u>98.30</u>	82.00	<u>5.40</u>
ParkingLot	Clear	99.20	<u>87.20</u>	4.20	94.80	51.50	21.50	95.60	62.00	20.00	<u>99.10</u>	88.00	3.80
	Adverse	98.90	<u>86.00</u>	4.80	94.00	50.50	23.00	95.10	61.00	21.00	<u>98.70</u>	87.00	4.20
Residential	Clear	99.20	<u>79.50</u>	2.40	94.60	52.50	20.80	95.30	62.00	20.20	<u>99.00</u>	80.20	<u>2.70</u>
	Adverse	98.90	<u>78.50</u>	2.80	94.20	51.00	22.00	95.00	61.00	21.00	<u>98.70</u>	79.50	<u>3.10</u>
Tunnel	Clear	97.40	<u>69.50</u>	9.80	91.80	40.00	35.00	93.00	52.00	28.00	<u>97.20</u>	70.50	<u>10.40</u>
	Adverse	97.00	<u>68.00</u>	10.50	91.00	38.00	37.00	92.50	51.00	29.00	<u>96.90</u>	69.00	<u>11.20</u>
Average	All	98.30	77.30	8.00	94.00	51.00	22.00	94.90	59.00	24.10	98.60	80.50	7.80

els trained on ClimaOoD better localize diverse anomalies, producing cleaner and more coherent anomaly maps than those trained on the baseline or clear-only data.

Overall, these results show that ClimaOoD substantially improves OoD robustness by providing richer environmental diversity and more realistic anomaly appearance.

4.4. Technical Analysis

Table 5 presents an analysis of the key components in the ClimaDrive framework. The goal of this analysis is to understand the contribution of each component to the overall performance in generating realistic OoD data. The perfor-

mance is evaluated using four key metrics: Fréchet Inception Distance (FID), Learned Perceptual Image Patch Similarity (LPIPS), and two Pearson Correlation Coefficients (PCC) based on entropy and max-logit scores, which measure the alignment between **generated data** and **real-world** OoD data from the SMIYC-RoadAnomaly21[6] benchmark, due to the similarity in object scale to our synthetic data. Specifically, entropy and max-logit are used to assess pixel-level uncertainty in model predictions.

The Full Model obtains the best results, with the lowest FID/LPIPS and highest PCC. Removing box supervision weakens physical alignment, and sparse sampling ($N =$

Table 4. Ablation study on training data for OoD detection. Metrics: AUROC (\uparrow), AP (\uparrow), FPR95 (\downarrow).

Method	Training Set	AUROC \uparrow	AP \uparrow	FPR95 \downarrow
<i>RoadAnomaly21</i>				
RbA[25]	Original	97.61	89.39	8.42
	Clear&City Street	97.83	90.15	7.96
	Full ClimaOoD	98.14	91.26	7.35
RPL[20]	Original	98.05	88.53	7.22
	Clear&City Street	98.28	89.77	6.85
	Full ClimaOoD	98.71	91.08	5.98
<i>RoadObstacle21</i>				
RbA[25]	Original	99.81	98.40	0.04
	Clear&City Street	99.84	98.27	0.06
	Full ClimaOoD	99.86	97.95	0.03
RPL[20]	Original	99.96	96.71	0.09
	Clear&City Street	99.80	96.93	0.15
	Full ClimaOoD	99.97	97.54	0.12

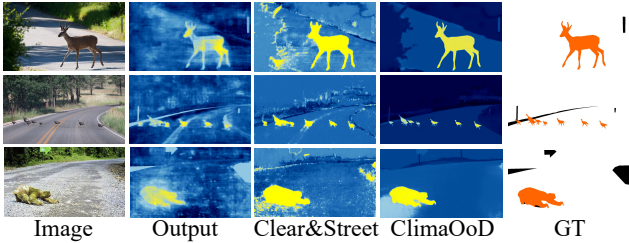


Figure 5. Visualization of Ablation Study for OoD Detection: RPL Outputs from Diverse Training Datasets (Left to Right: Image, Original RPL Output, Clear&Street-trained, ClimaOoD-trained, Ground Truth(GT))

Table 5. Ablation on the main components of ClimaDrive. Lower FID/LPIPS and higher PCC indicate better alignment with real OoD data.

Setting	FID \downarrow	LPIPS \downarrow	PCC \uparrow	
			entropy	max-logit
Full Model	175.2	0.276	0.86	0.87
w/o Box Supervision	191.3	0.293	0.78	0.80
w/o Joint Optimization	188.5	0.287	0.79	0.81
w/o Perspective Prior	190.2	0.291	0.77	0.79
Sparse Sampling ($N=32$)	183.9	0.282	0.80	0.82
Dense Sampling ($N=128$)	178.8	0.279	0.81	0.83

32) further degrades placement accuracy. Dense sampling ($N = 128$) improves the scores but still underperforms the full model. Overall, each component is necessary for generating physically consistent anomalies and achieving strong alignment with real OoD data.

Additional, we compare SD1.5[31], SD2[2], and SDXL[1] as inpainting backbones under the same training loss. Table 6 shows SDXL gives the best quality (FID=164.8, LPIPS=0.263) but is computationally heavy. SD2 achieves nearly the same realism with 40% fewer GFLOPs and is adopted as default.

Table 6. Comparison of diffusion backbones within ClimaDrive. SD2 balances quality and efficiency.

Backbone	Params (B)	GFLOPs	FID \downarrow	LPIPS \downarrow	PCC (\uparrow)	
					Entropy	Max-logit
SD1.5	0.89	185	186.5	0.291	0.72	0.74
SD2 (Default)	1.25	240	175.2	0.276	0.86	0.87
SDXL	2.60	410	164.8	0.263	0.88	0.89

Table 7. Different detection backbones in AnomPlacer. Results confirm geometric supervision.

Backbone	Params (B)	GFLOPs	FID \downarrow	LPIPS \downarrow	PCC (\uparrow)	
					Entropy	Max-logit
DETR (ResNet-50)	1.20	250	178.4	0.279	0.84	0.85
DINO (Swin-B)	1.25	240	175.2	0.276	0.86	0.87

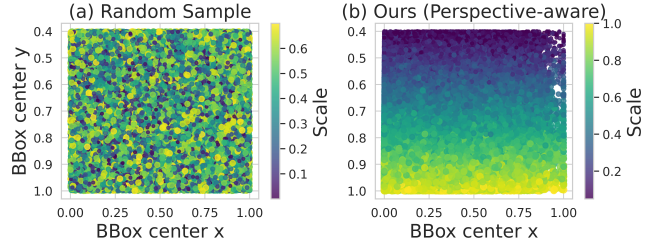


Figure 6. Comparison of box distributions shows that random sampling leads to scattered placements, while our perspective-aware sampling creates a natural depth-size pattern, enhancing anomaly location prediction.

To verify universality, we replace the detection module with DETR[4]-ResNet50 and DINO[42]-Swin-B, trained jointly with SD2. As shown in Table 7, DETR yields FID=178.4 and PCC_{entropy}=0.84, while DINO slightly improves to 175.2 and 0.86. The difference across all metrics is under 2%, confirming stable performance across architectures.

As shown in Figure 6, random sampling produces physically implausible placements, with box locations and scales showing no spatial correlation. In contrast, our perspective-aware sampling enforces a natural depth-size relationship, where boxes closer to the ego-vehicle appear larger. This simple geometric prior provides an effective pseudo-supervision signal, enabling more realistic and consistent anomaly placement without extra annotations.

5. Conclusion

In this work, we introduce ClimaOoD, a comprehensive benchmark with over 10,000 high-quality image-mask pairs across six driving scenarios and various weather conditions, enabling robust anomaly segmentation evaluation. ClimaDrive, our proposed framework, integrates AnomPlacer for consistent object placement and a weather generator for diverse environmental synthesis. Experiments show that training with ClimaOoD improves model performance, highlighting its effectiveness in enhancing precision and recall in anomaly segmentation.

References

- [1] Stability AI. Sdxl: Improving latent diffusion models for high-resolution image synthesis. In *CoRR*, 2023. 8
- [2] Stability AI. stable-diffusion-2-inpainting model card. <https://huggingface.co/stabilityai/stable-diffusion-2-inpainting>, 2023. 8
- [3] Hermann Blum, Paul-Edouard Sarlin, Juan Nieto, Roland Siegwart, and Cesar Cadena. The fishyscapes benchmark: Measuring blind spots in semantic segmentation. *International Journal of Computer Vision*, 129(11):3119–3135, 2021. 2, 3, 4, 5
- [4] Nicolas Carion, Francisco Massa, Gabriel Synnaeve, Nicolas Usunier, Alexander Kirillov, and Sergey Zagoruyko. End-to-end object detection with transformers. In *Proceedings of the European Conference on Computer Vision*, pages 213–229, 2020. 8
- [5] Robin Chan, Matthias Rottmann, and Hanno Gottschalk. Entropy maximization and meta classification for out-of-distribution detection in semantic segmentation. In *Proceedings of the IEEE International Conference on Computer Vision*, pages 5128–5137, 2021. 2
- [6] Robin Kien-Wei Chan, Krzysztof Lis, Svenja Uhlemeyer, Hermann Blum, Sina Honari, Roland Siegwart, Pascal Fua, Mathieu Salzmann, and Matthias Rottmann. Segmentneifyoucan: A benchmark for anomaly segmentation. In *Proceedings of the Advances in Neural Information Processing Systems*, pages 24124–24136, 2021. 2, 3, 4, 5, 7
- [7] Liang-Chieh Chen, Yukun Zhu, George Papandreou, Florian Schroff, and Hartwig Adam. Encoder-decoder with atrous separable convolution for semantic image segmentation. In *Proceedings of the European Conference on Computer Vision*, page 2, 2018. 1
- [8] Xuesong Chen, Linjiang Huang, Tao Ma, Rongyao Fang, Shaoshuai Shi, and Hongsheng Li. Solve: Synergy of language-vision and end-to-end networks for autonomous driving. In *CoRR*, 2025. 2
- [9] Marius Cordts, Mohamed Omran, Sebastian Ramos, Timo Rehfeld, Markus Enzweiler, Rodrigo Benenson, Uwe Franke, Stefan Roth, and Bernt Schiele. The cityscapes dataset for semantic urban scene understanding. In *Proceedings of the IEEE Conference on Computer Vision and Pattern Recognition*, 2016. 2, 3
- [10] Anja Delić, Matej Grcić, and Siniša Šegvić. Outlier detection by ensembling uncertainty with negative objectness. In *CoRR*, 2024. 2, 5, 7
- [11] Giancarlo Di Biase, Hermann Blum, Roland Y. Siegwart, and César Cadena. Pixel-wise anomaly detection in complex driving scenes. In *Proceedings of the IEEE Conference on Computer Vision and Pattern Recognition*, 2021. 2
- [12] Franck Djeumou, Thomas Jonathan Lew, Nan Ding, Michael Thompson, Makoto Suminaka, Marcus Greiff, and John Subosits. One model to drift them all: Physics-informed conditional diffusion model for driving at the limits. In *Conference on Robot Learning*, pages 604–630, 2025. 2
- [13] Jonathan Ho, Ajay Jain, and Pieter Abbeel. Denoising diffusion probabilistic models. *arXiv preprint arXiv:2006.11239*, 2020. 1
- [14] Daehyun Kim, Sungyong Baik, and Tae Hyun Kim. Sanflow: Semantic-aware normalizing flow for anomaly detection and localization. In *Proceedings of the Advances in Neural Information Processing Systems*, pages 25681–25693, 2023. 3
- [15] Junnan Li, Xi Yin, Chunyuan Li, and Steven C.H. Hoi. Blip: Bootstrapping language-image pre-training for unified vision-language understanding and generation. In *Proceedings of the International Conference on Machine Learning*, 2022. 3, 1
- [16] Youwei Liang, Junfeng He, Gang Li, Peizhao Li, Arseniy Klimovskiy, Nicholas Carolan, Jiao Sun, Jordi Pont-Tuset, Sarah Young, and Feng Yang. Rich human feedback for text-to-image generation. In *Proceedings of the IEEE Conference on Computer Vision and Pattern Recognition*, 2024. 3
- [17] Tsung-Yi Lin, Michael Maire, Serge Belongie, James Hays, Pietro Perona, Deva Ramanan, Piotr Dollár, and C Lawrence Zitnick. Microsoft coco: Common objects in context. In *Proceedings of the European Conference on Computer Vision*, pages 740–755. Springer, 2014. 2
- [18] Krzysztof Lis, Krishna Nakka, Pascal Fua, and Mathieu Salzmann. Detecting the unexpected via image resynthesis. In *Proceedings of the IEEE International Conference on Computer Vision*, pages 2152–2161, 2019. 2, 3, 4, 5
- [19] Krzysztof Lis, Sina Honari, Pascal Fua, and Mathieu Salzmann. Detecting road obstacles by erasing them. In *CoRR*, 2020. 3
- [20] Yuyuan Liu, Choubo Ding, Yu Tian, Guansong Pang, Vasileios Belagiannis, Ian Reid, and Gustavo Carneiro. Residual pattern learning for pixel-wise out-of-distribution detection in semantic segmentation. In *Proceedings of the IEEE International Conference on Computer Vision*, pages 1151–1161, 2023. 2, 3, 5, 7, 8
- [21] Yuxing Liu, Ji Zhang, Xuchuan Zhou, Jingzhong Xiao, Huimin Yang, and Jiaxin Zhong. Ooddino: A multi-level framework for anomaly segmentation on complex road scenes. *Proceedings of the ACM International Conference on Multimedia*, 2025. 3
- [22] Thibaut Loiseau, Tuan-Hung Vu, Mickael Chen, Patrick Pérez, and Matthieu Cord. Reliability in semantic segmentation: Can we use synthetic data? In *Proceedings of the European Conference on Computer Vision*, pages 442–459. Springer, 2024. 2, 3, 1
- [23] Ilya Loshchilov and Frank Hutter. Decoupled weight decay regularization. In *Proceedings of the International Conference on Learning Representations*, 2018. 1
- [24] Lvmin Lv, Mingsheng Zhang, et al. Controlnet: Adding conditional control to text-to-image diffusion models. In *CoRR*, 2023. 3, 1
- [25] Nazir Nayal, Misra Yavuz, Joao F Henriques, and Fatma Güney. Rba: Segmenting unknown regions rejected by all. In *Proceedings of the IEEE International Conference on Computer Vision*, pages 711–722, 2023. 2, 3, 5, 7, 8
- [26] Alexey Nekrasov, Malcolm Burdorf, Stewart Worrall, Bastian Leibe, and Julie Stephany Berrio Perez. Spotting the unexpected (stu): A 3d lidar dataset for anomaly segmentation in autonomous driving. In *Proceedings of the IEEE Conference on Computer Vision and Pattern Recognition*, page 33129, 2025. 2

- [27] Weili Nie, Sifei Liu, Morteza Mardani, Chao Liu, Benjamin Eckart, and Arash Vahdat. Compositional text-to-image generation with dense blob representations. In *Proceedings of the International Conference on Machine Learning*, 2024. 3
- [28] Marianna Ohanyan, Hayk Manukyan, Zhangyang Wang, Shant Navasardyan, and Humphrey Shi. Zero-painter: Training-free layout control for text-to-image synthesis. In *Proceedings of the IEEE Conference on Computer Vision and Pattern Recognition*, 2024. 3
- [29] Peter Pinggera, Sebastian Ramos, Stefan Gehrig, Uwe Franke, Carsten Rother, and Rudolf Mester. Lost and found: Detecting small road hazards for self-driving vehicles. In *CoRR*, 2016. 2, 3, 4
- [30] Shyam Nandan Rai, Fabio Cermelli, Barbara Caputo, and Carlo Masone. Mask2anomaly: Mask transformer for universal open-set segmentation. *IEEE Transactions on Pattern Analysis and Machine Intelligence*, 2024. 2, 5, 7
- [31] Robin Rombach, Andreas Blattmann, Dominik Lorenz, Patrick Esser, and Björn Ommer. High-resolution image synthesis with latent diffusion models. In *Proceedings of the IEEE Conference on Computer Vision and Pattern Recognition*, 2022. 8
- [32] Robin Rombach, Andreas Blattmann, Dominik Lorenz, Patrick Esser, and Björn Ommer. High-resolution image synthesis with latent diffusion models. In *Proceedings of the IEEE Conference on Computer Vision and Pattern Recognition*, pages 10684–10695, 2022. 3
- [33] Youssef Shoeb, Azarm Nowzad, and Hanno Gottschalk. Out-of-distribution segmentation in autonomous driving: Problems and state of the art. In *CoRR*, 2025. 3
- [34] Jacob Steinhardt and Dawn Song. A benchmark for anomaly segmentation. In *CoRR*, 2019. 3
- [35] Han Sun, Yunkang Cao, Hao Dong, and Olga Fink. Anomalyany: Promptable unseen visual anomaly generation. In *Proceedings of the IEEE Conference on Computer Vision and Pattern Recognition*, pages 12456–12467, 2025. 3
- [36] Yu Tian, Yuyuan Liu, Guansong Pang, Fengbei Liu, Yuanhong Chen, and Gustavo Carneiro. Pixel-wise energy-biased abstention learning for anomaly segmentation on complex urban driving scenes. In *Proceedings of the European Conference on Computer Vision*, 2022. 3
- [37] Tomas Vojir, Tomáš Šipka, Rahaf Aljundi, Nikolay Chumerin, Daniel Olmeda Reino, and Jiri Matas. Rsj international conference on intelligent robots and systems. In *Proceedings of the IEEE International Conference on Computer Vision*, 2021. 3
- [38] Song Xia, Yi Yu, Henghui Ding, Wenhan Yang, Shifei Liu, Alex C. Kot, and Xudong Jiang. Open-set anomaly segmentation in complex scenarios. In *CoRR*, 2025. 2, 3
- [39] Enze Xie, Wenhai Wang, Zhiding Yu, Anima Anandkumar, Jose M Alvarez, and Ping Luo. Segformer: Simple and efficient design for semantic segmentation with transformers. *Proceedings of the Advances in Neural Information Processing Systems*, 34, 2021. 1
- [40] Yi Xu, Yuxin Hu, Zaiwei Zhang, Gregory P. Meyer, Siva Karthik Mustikovela, Siddhartha Srinivasa, Eric M. Wolff, and Xin Huang. Vlm-ad: End-to-end autonomous driving through vision-language model supervision. In *International Conference on Robotics and Automation*, pages 1–9, 2025. 2
- [41] Fisher Yu, Haofeng Chen, Xin Wang, Wenqi Xian, Yingying Chen, Fangchen Liu, Vashisht Madhavan, and Trevor Darrell. Bdd100k: A diverse driving dataset for heterogeneous multitask learning. In *Proceedings of the IEEE Conference on Computer Vision and Pattern Recognition*, 2020. 3, 1
- [42] Hao Zhang, Feng Li, Shilong Liu, Lei Zhang, Hang Su, Jun Zhu, Lionel M. Ni, and Heung-Yeung Shum. Dino: Detr with improved denoising anchor boxes for end-to-end object detection. In *CoRR*, 2022. 8
- [43] Ji Zhang, Xiao Wu, Zhi-Qi Cheng, Qi He, and Wei Li. Improving anomaly segmentation with multi-granularity cross-domain alignment. In *Proceedings of the ACM International Conference on Multimedia*, pages 8515–8524, 2023. 2, 3
- [44] Hengshuang Zhao, Jianping Shi, Xiaojuan Qi, Xiaogang Wang, and Jiaya Jia. Pyramid scene parsing network. In *Proceedings of the IEEE Conference on Computer Vision and Pattern Recognition*, page 2, 2017. 1
- [45] Wenjie Zhao, Jia Li, Xin Dong, Yu Xiang, and Yunhui Guo. Segment every out-of-distribution object. In *Proceedings of the IEEE Conference on Computer Vision and Pattern Recognition*, pages 3910–3920, 2024. 2, 3
- [46] Mi Zheng, Guanglei Yang, Zitong Huang, Zhenhua Guo, Kevin Han, and Wangmeng Zuo. Segmenting objectiveness and task-awareness unknown region for autonomous driving. *Proceedings of the ACM International Conference on Multimedia*, 2025. 3
- [47] Bolei Zhou, Hang Zhao, Xavier Puig, Sanja Fidler, Adela Barriuso, and Antonio Torralba. Semantic understanding of scenes through the ade20k dataset. *International Journal of Computer Vision*, 127(2):302–321, 2019. 2
- [48] Qiang Zhou, Weize Li, Lihan Jiang, Guoliang Wang, Guyue Zhou, Shanghang Zhang, and Hao Zhao. Pad: A dataset and benchmark for pose-agnostic anomaly detection. In *Proceedings of the Advances in Neural Information Processing Systems*, pages 7890–7901, 2023. 3
- [49] Siyuan Zhu, Pengtao Zhang, Peize Sun, Jiacheng Liu, Xiaolong Wang, Junnan Li, Jiashi Feng, Tong Zhou, Xiyang Dai, Yici Cai, et al. Grounded sam: Assembling open-world models for diverse visual tasks. In *CoRR*, 2024. 4

ClimaOoD: Improving Anomaly Segmentation via Physically Realistic Synthetic Data

Supplementary Material

Supplementary Material

This supplementary document provides additional implementation details, extended experiments, and qualitative results complementing the main paper.

The supplementary content is organized as follows:

- **Section 5.1** — Details of the inference pipeline, including multi-weather scene generation and AnomPlacer-based OoD object placement.
- **Section 5.2** — Implementation details and text prompt design for guided scene generation.
- **Section 5.3** — In-domain evaluation of semantic consistency between synthetic and training data.
- **Section 5.4** — Quantitative analysis of correlation between uncertainty metrics (e.g., max-logit, entropy).
- **Section 5.5** — Cross-dataset correlation analysis of uncertainty metric generalizability.
- **Section 5.6** — Enumeration of five categories of OoD objects for experiments.
- **Section 5.7** — Cross-dataset generalization analysis on Cityscapes.
- **Section 5.8** — Formal definitions of evaluation metrics (e.g., mIoU, PCC) for reproducibility.
- **Section 5.9** — Principles and roles of entropy and max-logit uncertainty.

5.1. Inference Pipeline

During inference, ClimaOoD operates through a two-stage generation process, as illustrated in Figure 8. Given an input semantic map, the in-domain multi-weather generator first produces structure-consistent scenes under user-specified environmental conditions. These synthesized scenes are then processed by AnomPlacer, which inserts anomalous objects using detection-guided diffusion, ensuring realistic geometry, scale, and contextual alignment. This pipeline enables controllable scene synthesis and coherent OoD object placement, forming a reliable basis for training and evaluating anomaly segmentation models.

5.2. Implementation Details and Prompt Construction

semantics-guided model Pretraining. We fine-tune a semantics-guided image-to-image framework, implemented with a ControlNet[24]-style conditioning branch, on top of a frozen Stable Diffusion backbone [13] using the BDD100K [41] dataset for 100 epochs. Semantic segmentation masks serve as conditions, and captions generated by BLIP [15] provide textual guidance. Images are randomly

cropped and resized to 512×512 . The learning rate is set to 1×10^{-5} , batch size is 2, and gradient accumulation is 8.

Two-Stage Optimization of AnomPlacer. Training is performed in two stages: *Stage 1*: A detection backbone is trained with perspective-aware box supervision using 64 object queries and the AdamW[23] optimizer (1×10^{-4} learning rate). *Stage 2*: The detector and diffusion-based inpainting model are jointly optimized for 25 epochs with a learning rate of 1×10^{-5} , refining pseudo-anomalies using prompts sampled from 93 curated OoD object categories.

Prompt Construction. Prompts are automatically assembled from scene descriptors extracted via BLIP captions, which include attributes such as weather, time of day, and scene type. The final prompt takes the form: "{OoD_object} in {scene_descriptor}, high quality, detailed" (e.g., "traffic cone in city street, rainy, daytime"). Negative prompts ("blurry, distorted, unrealistic") are consistently applied to suppress artifacts.

Inference-time Prompt Assembly. During inference, prompts are dynamically generated from user-defined attributes (weather, time, scene), enabling controllable scene generation. The structure-guided diffusion model uses conditioning strength of 0.65, guidance scale of 10, and 25 DDIM steps to maintain structural fidelity.

5.3. In-domain Synthetic Evaluation

A crucial requirement of synthetic data is maintaining semantic fidelity to real-world distributions. Beyond generating OoD objects, our framework synthesizes large-scale in-domain driving data under diverse weather and scene conditions using a diffusion-based generator. Verifying semantic consistency ensures that these samples provide valid supervision for downstream models.

Evaluation Protocol. We adopt three representative semantic segmentation models—DeepLabV3+ [7], PSPNet [44], and SegFormer [39]—pretrained on BDD100K [41]. Each model is evaluated on both real and synthetic datasets using: *Per-class IoU*, capturing class-wise consistency; *Pearson Correlation Coefficient (PCC)* [22], measuring the correlation between mIoU values on real and synthetic domains.

Results and Analysis. Figure 7 (top) reports per-class IoU across the three backbones. Major classes such as *road*, *building*, *sky*, and *car* maintain strong consistency, while minor categories (e.g., *traffic light*, *pole*) show moderate drops due to texture-level complexity. As shown in Fig. 7

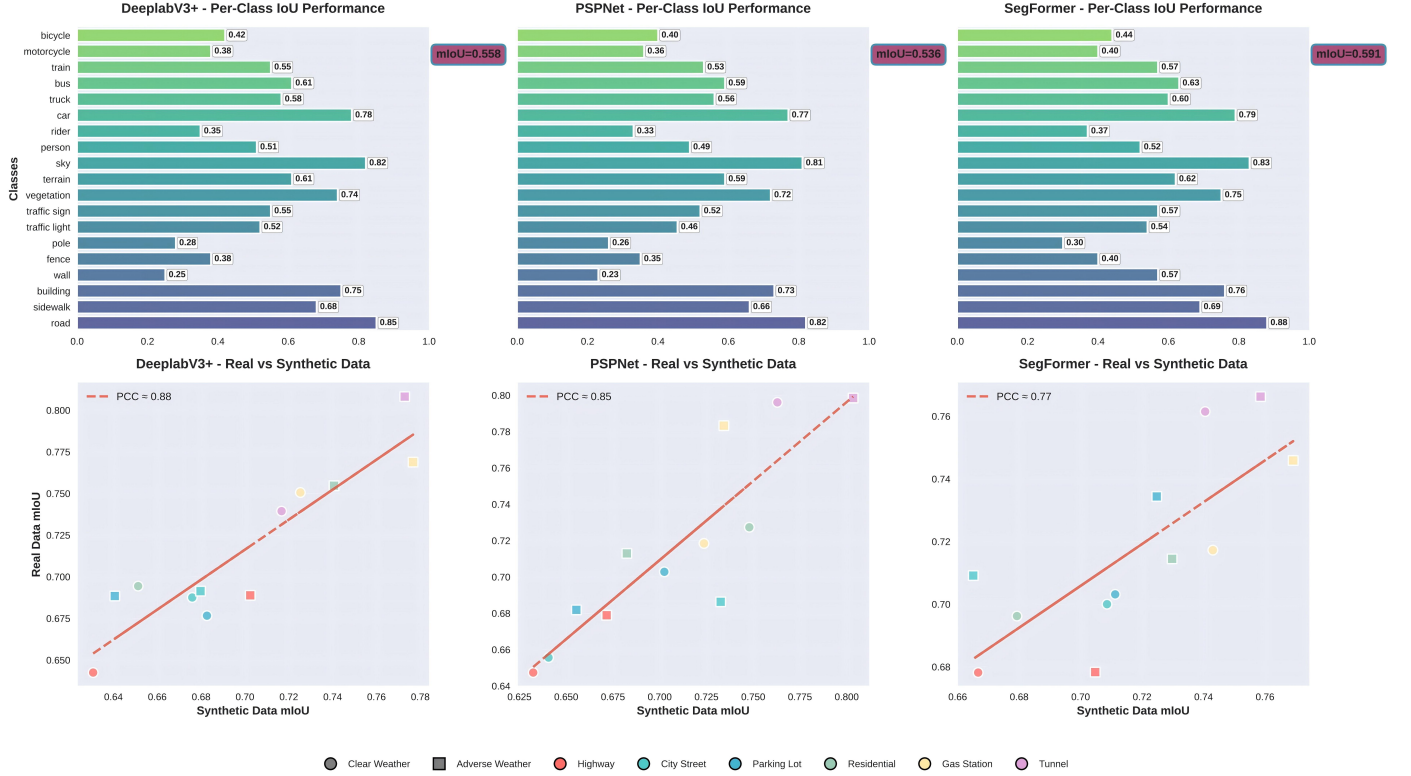


Figure 7. In-domain synthetic evaluation. **Top:** Per-class IoU of three segmentation backbones, showing consistent semantic structure across real and synthetic domains. **Bottom:** Correlation between real and synthetic mIoU across scene/weather conditions. High PCC scores confirm semantic fidelity of synthetic data.

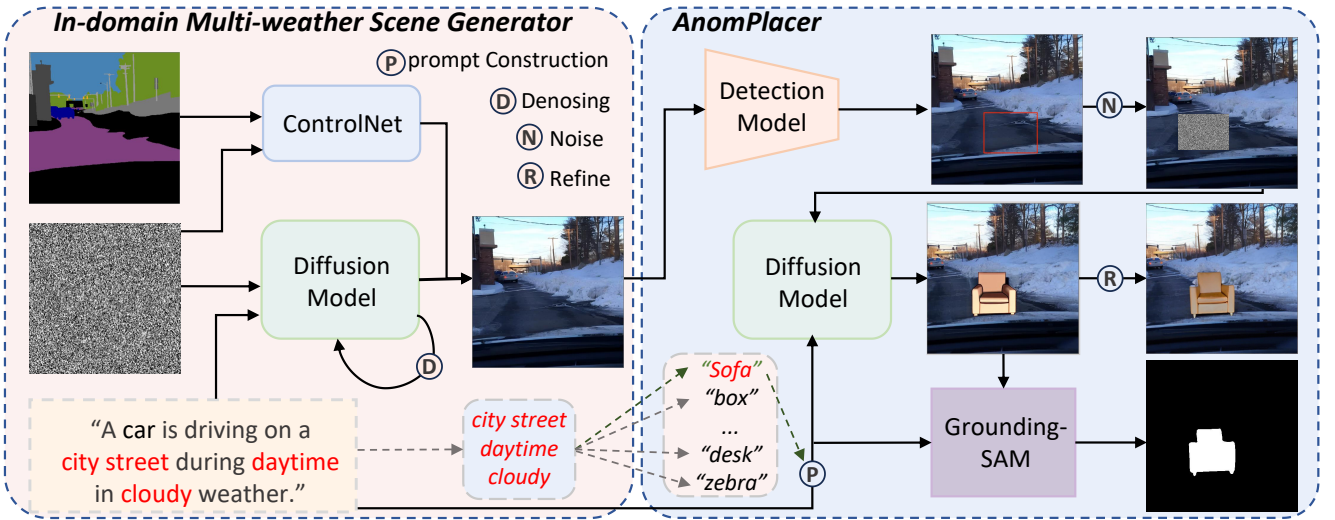


Figure 8. **Inference pipeline of the ClimaOoD framework.** Our method consists of two complementary components: (1) **In-domain Multi-weather Scene Generator**, which leverages a structure-guided diffusion model to generate diverse, weather-consistent driving scenes from semantic maps under multiple environmental conditions; and (2) **AnomPlacer**, which employs a detection-guided diffusion process to insert out-of-distribution (OoD) objects with realistic scale, perspective, and semantic plausibility.

(bottom), the mIoU correlation between synthetic and real domains is high, achieving PCC scores of 0.88, 0.85, and

0.77 for DeepLabV3+, PSPNet, and SegFormer, respectively. These results verify that our diffusion model preserves global semantics and structural layout, even under large appearance shifts such as weather and illumination changes. Hence, ClimaOoD provides reliable and semantically consistent synthetic supervision for segmentation.

5.4. Calculation of PCC Between Uncertainty Metrics

To quantify the correlation between uncertainty metrics (max-logit and entropy) of real and synthetic data, we compute the Pearson Correlation Coefficient (PCC), as shown in Figure 9.

For both synthetic and real scenes, we use pretrained semantic segmentation models to obtain logits for each pixel. For **max-logit**, we calculate the maximum logit value across all classes for each pixel. For **entropy**, we first convert logits to class probabilities using softmax, then compute the entropy for each pixel as the negative sum of $p_{i,j}^c \log(p_{i,j}^c)$, where $p_{i,j}^c$ is the probability for class c . We add a small epsilon (10^{-8}) to avoid numerical issues.

After obtaining the max-logit and entropy maps for both datasets, we flatten them into one-dimensional arrays ($\mathbf{M}_{\text{synthetic}}, \mathbf{E}_{\text{synthetic}}$ for synthetic data, and $\mathbf{M}_{\text{real}}, \mathbf{E}_{\text{real}}$ for real data). Finally, we compute the PCC between corresponding uncertainty maps, with higher values indicating stronger correlation between synthetic and real data uncertainty metrics.

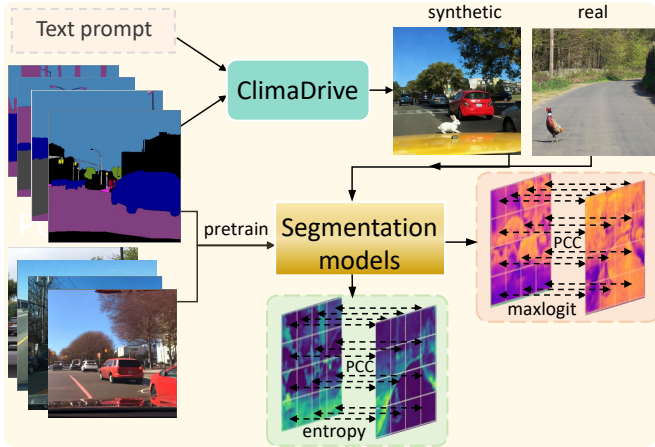


Figure 9. Visualization of Pearson Correlation Coefficient (PCC) calculation between uncertainty values of real and synthetic data. ClimaOoD generates synthetic scenes using text prompts and semantic maps. Pretrained segmentation models compute *max-logit* (model confidence) and *entropy* (uncertainty) for both datasets, and PCC quantifies their correlation.

Table 8. Cross-dataset correlation analysis between synthetic ClimaDrive data and real OoD datasets. Higher PCC values indicate stronger alignment in uncertainty responses and scene structure.

Dataset Pair	PCC \uparrow	
	Entropy	Max-logit
ClimaOoD – RoadAnomaly [18]	0.72	0.74
ClimaOoD – FishyScapes L&F [3]	0.70	0.71
RoadAnomaly – FishyScapes L&F (real-to-real)	0.78	0.79

5.5. Cross-Dataset Correlation Analysis

To further validate the realism and uncertainty consistency of our generated anomalies, we conduct a cross-dataset correlation analysis between ClimaDrive and real-world OoD benchmarks, including **SMIYC-RoadAnomaly21**[6] and **FishyScapes Lost&Found**[3]. We use a pretrained SegFormer-B2 model to extract pixel-level confidence responses on both datasets and compute two correlation metrics: PCC_{entropy} and $PCC_{\text{max-logit}}$. Both metrics are computed across aligned scenes and averaged over the validation split.

Analysis. As shown in Table 8, ClimaDrive maintains a moderate yet stable correlation with real-world OoD datasets ($PCC_{\text{entropy}} = 0.7$, $PCC_{\text{max-logit}} = 0.73$), indicating that the generated anomalies exhibit comparable uncertainty patterns to real outliers. The correlation gap with the real-to-real comparison is expected, as real datasets contain naturally complex distributions and noise. Nevertheless, the results demonstrate that ClimaDrive effectively approximates real OoD uncertainty characteristics, suggesting strong transferability of synthetic anomalies for benchmarking OoD detection models.

5.6. OoD Objects List

To ensure comprehensive evaluation of out-of-distribution (OoD) detection performance, we define five categories of typical OoD objects commonly encountered in road scenes, as listed in Table 9. These objects cover animals, non-standard vehicles, road facilities, daily items, and sports equipment, which are distinct from the normal traffic elements in training datasets and thus serve as representative OoD samples for our experiments.

5.7. Cross-Dataset Generalization.

We test zero-shot transfer by applying the BDD100K-trained model to Cityscapes [9] without finetuning, compared with the Fishyscapes (Static) copy-paste baseline [3]. Table 10 shows clear improvement, demonstrating strong cross-domain realism and robustness.

AnomPlacer generalizes well across domains: when trained only on BDD100K and directly applied to Cityscapes (Figure 10), it maintains realistic geometry and context, demonstrating strong zero-shot transferability.

Category	Items
Animals	dog, cat, deer, rabbit, squirrel, bird, duck, goose, chicken, cow, horse, sheep, goat, pig, fox, raccoon, opossum, skunk, bear, moose, elk, bison, llama, alpaca, donkey, mule, camel, elephant, zebra, giraffe, lion, tiger, leopard, cheetah, wolf, coyote, hyena, kangaroo, koala, panda
Vehicles	motorcycle, bicycle, scooter, skateboard, rollerblades, wheelchair, stroller, shopping_cart, wheelbarrow, golf_cart, snowmobile, jet_ski, hoverboard, segway, unicycle
Road Facilities	traffic_cone, road_barrier, construction_sign, speed_bump, manhole_cover, drain_cover, fire_hydrant, mailbox, trash_can, recycling_bin, bench, bus_stop, phone_booth, atm_machine, vending_machine
Items	backpack, suitcase, paper_bag, grocery_bag, umbrella, ladder, toolbox, generator, air_conditioner, refrigerator, washing_machine, dryer, portable_toilet
Sports Equipment	basketball, football, soccer_ball, tennis_ball, baseball, golf_ball, frisbee, kite, balloon, toy_car

Table 9. OoD objects list table.

Table 10. Cross-dataset evaluation on Cityscapes. The BDD100K-trained model generalizes well without finetuning.

Method	FID ↓	LPIPS ↓
Fishyscapes (Static)	214.6	0.342
Ours (zero-shot)	182.7	0.281

5.8. Metric Formulations

We adopt standard quantitative metrics for anomaly segmentation and generative modeling. Below we provide formal definitions used in our experiments.

Anomaly detection metrics. Let $y_i \in \{0, 1\}$ be the ground-truth label of pixel i (1 = anomaly), and $s_i \in \mathbb{R}$ the predicted anomaly score for pixel i . Denote by \mathcal{I} the set of all pixels and by $N = |\mathcal{I}|$.

- **AUROC:** Area under the Receiver Operating Characteristic curve. If $\text{TPR}(t)$ and $\text{FPR}(t)$ denote true- and false-positive rates at threshold t , then

$$\text{AUROC} = \int_0^1 \text{TPR}(\text{FPR}^{-1}(u)) du$$

In practice we compute AUROC from the empirical ROC curve obtained by sorting scores s_i and applying the trapezoidal rule.

- **AP** Area under the precision–recall curve (positive class as anomaly). Let precision $P(t)$ and recall $R(t)$ be at

threshold t . Then

$$\text{AP} = \int_0^1 P(R^{-1}(r)) dr,$$

which is computed empirically from the discrete precision–recall points (trapezoidal or Riemann-sum approximation).

- **FPR95:** False Positive Rate when True Positive Rate = 95%. Formally

$$\text{FPR95} = \min_t \{\text{FPR}(t) \mid \text{TPR}(t) \geq 0.95\}.$$

Lower FPR95 is better for safety-critical applications.

Image quality and alignment metrics. Let $\{x_k\}_{k=1}^{M_r}$ be features of M_r real images and $\{\hat{x}_k\}_{k=1}^{M_g}$ be features of M_g generated images, where features are extracted by a pretrained network (Inception for FID). Denote μ_r, Σ_r and μ_g, Σ_g the empirical means and covariances of real and generated features, respectively.

- **FID (Fréchet Inception Distance):** measures distance between two Gaussian approximations of feature distributions:

$$\text{FID} = \|\mu_r - \mu_g\|_2^2 + \text{Tr}(\Sigma_r + \Sigma_g - 2(\Sigma_r \Sigma_g)^{1/2}).$$

Lower FID indicates closer distributional similarity between real and generated images.

- **LPIPS (Learned Perceptual Image Patch Similarity):** for an image pair (x, \hat{x}) , LPIPS compares multi-layer

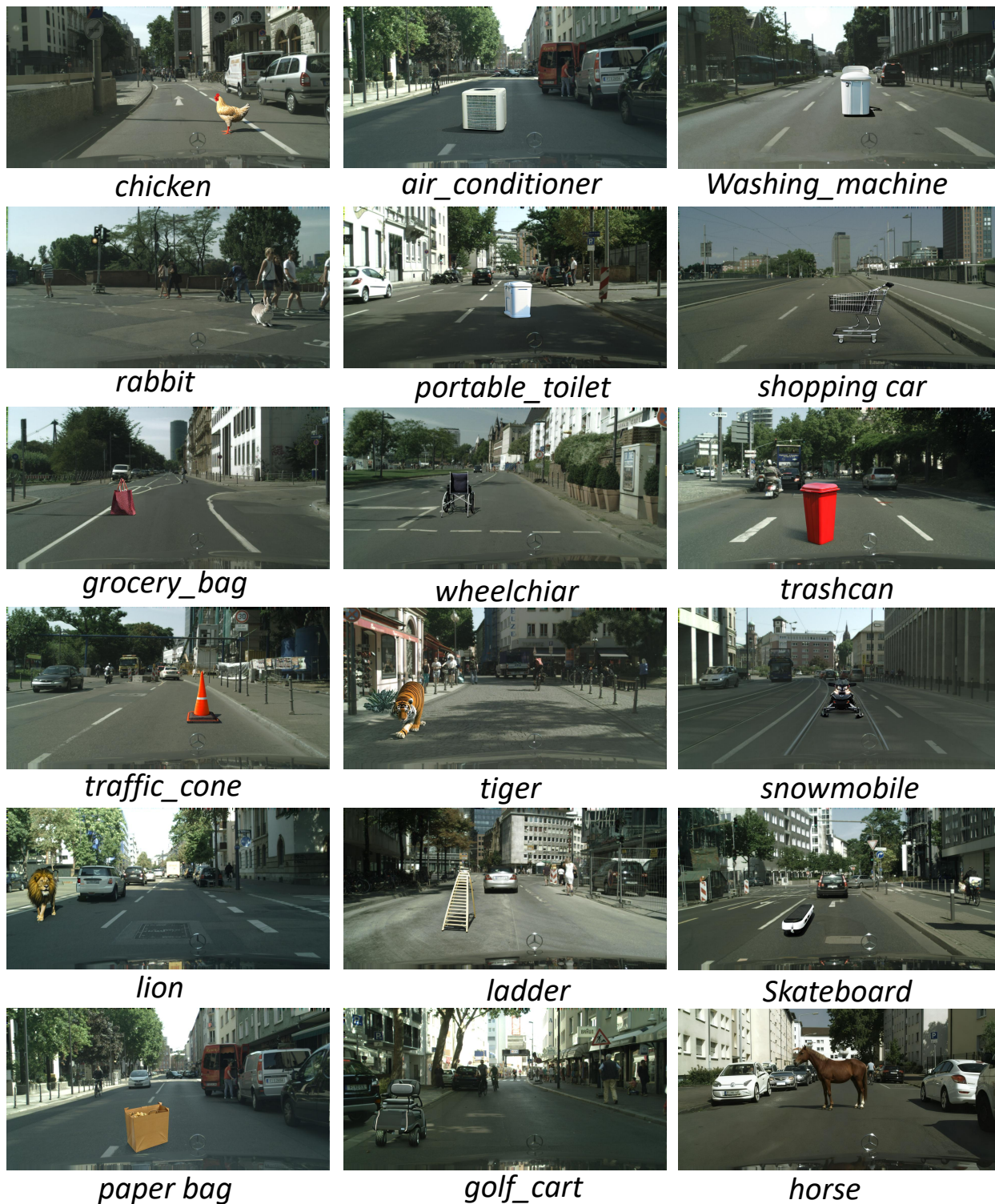


Figure 10. **Zero-shot anomaly placement on Cityscapes.** Examples of **AnomPlacer** trained on BDD100K and applied directly to Cityscapes without finetuning. The model effectively generates semantically coherent anomalies (e.g., animals, objects, and vehicles) with proper perspective and scene alignment, demonstrating strong cross-dataset generalization.

deep activations. Let $\phi_l(\cdot) \in \mathbb{R}^{C_l \times H_l \times W_l}$ be activations at layer l , and let w_l be learned layer weights. Then

$$\text{LPIPS}(x, \hat{x}) = \sum_l w_l \cdot \frac{1}{H_l W_l} \sum_{h,w} \|\tilde{\phi}_l(x)_{h,w} - \tilde{\phi}_l(\hat{x})_{h,w}\|_2$$

where $\tilde{\phi}_l$ denotes channel-wise normalized activations. Reported LPIPS is the average over image pairs; lower is more perceptually similar.

- **PCC (Pearson Correlation Coefficient):** used to measure structural alignment between two maps (e.g., uncertainty score maps or per-image scalar responses). For two vectors $a = (a_i)_{i=1}^n$ and $b = (b_i)_{i=1}^n$,

$$\text{PCC}(a, b) = \frac{\sum_{i=1}^n (a_i - \bar{a})(b_i - \bar{b})}{\sqrt{\sum_{i=1}^n (a_i - \bar{a})^2} \sqrt{\sum_{i=1}^n (b_i - \bar{b})^2}},$$

where \bar{a} and \bar{b} are means. In our experiments PCC is computed between score maps (or aggregated per-image scores) of *real* OoD samples and *synthetic* OoD samples using a pretrained SegFormer model: higher PCC implies stronger agreement in uncertainty response patterns.

5.9. Entropy and Max-Logit Uncertainty

Uncertainty estimation is a fundamental component in OoD segmentation, as it provides a quantitative measure of how confident a model is about its pixel-wise predictions. In our experiments, we adopt two widely used uncertainty formulations: **entropy-based** and **max-logit-based** uncertainty. Both are computed from the softmax output $\mathbf{p} \in \mathbb{R}^K$ of a segmentation model over K classes.

Entropy-based Uncertainty. Entropy quantifies the amount of disorder or uncertainty in the predicted class distribution:

$$U_{\text{entropy}}(x) = - \sum_{k=1}^K p_k(x) \log p_k(x), \quad (1)$$

where $p_k(x)$ denotes the predicted probability for class k at pixel x . Higher entropy indicates more ambiguous predictions, often corresponding to pixels belonging to anomalies or unseen regions.

Max-Logit-based Uncertainty. Instead of using the full probability distribution, the max-logit approach directly leverages the pre-softmax logits \mathbf{z} to estimate confidence:

$$U_{\text{max-logit}}(x) = - \max_k z_k(x), \quad (2)$$

where $z_k(x)$ is the logit for class k at pixel x . A lower maximum logit value (hence higher negative score) implies greater uncertainty. This metric has been shown to better capture overconfidence issues in deep networks by avoiding softmax saturation effects.

Interpretation and Usage. In practice, both measures produce uncertainty maps that highlight anomalous or ambiguous regions. Entropy emphasizes distributional ambiguity, while max-logit focuses on absolute confidence suppression. As demonstrated in our experiments, both correlate well with real OoD uncertainty patterns — with $\text{PCC}_{\text{entropy}} = 0.86$ and $\text{PCC}_{\text{max-logit}} = 0.87$ for our full model — indicating that ClimaDrive-generated data effectively reproduces the uncertainty behavior observed in real anomaly segmentation benchmarks.